Preclinical validation of the advection diffusion flow estimation method using computational patient specific coronary tree phantoms

Received: 28 December 2022 | Revised: 24 March 2023 | Accepted: 11 June 2023

DOI: 10.1002/cnm.3746

APPLIED RESEARCH

WILEY

Preclinical validation of the advection diffusion flow estimation method using computational patient specific coronary tree phantoms

L. M. M. L. Bakker[1] | **N. Xiao**[2] | **S. Lynch**[2] | **A. A. F. van de Ven**[3] | **A. UpdePac**[2] | **M. Schaap**[2] | **N. Buls**[4] | **J. de Mey**[4] | **F. N. van de Vosse**[1] | **C. A. Taylor**[1,2]

[1]Department of Biomedical Engineering, Eindhoven University of Technology, Eindhoven, The Netherlands

[2]HeartFlow, Inc., Mountain View, California, USA

[3]Department of Mathematics and Computer Science, Eindhoven University of Technology, Eindhoven, The Netherlands

[4]Department of Radiology, Vrije Universiteit Brussel, Universitair Ziekenhuis Brussel, Jette, Belgium

Correspondence
L. M. M. L. Bakker, Eindhoven University of Technology, 5600MB Eindhoven, The Netherlands.
Email: l.m.m.l.bakker@tue.nl

Funding information
HeartFlow, Inc.

Abstract

Coronary computed tomography angiography (CCTA) does not allow the quantification of reduced blood flow due to coronary artery disease (CAD). In response, numerical methods based on the CCTA image have been developed to compute coronary blood flow and assess the impact of disease. However to compute blood flow in the coronary arteries, numerical methods require specification of boundary conditions that are difficult to estimate accurately in a patient-specific manner. We describe herein a new noninvasive flow estimation method, called Advection Diffusion Flow Estimation (ADFE), to compute coronary artery flow from CCTA to use as boundary conditions for numerical models of coronary blood flow. ADFE uses image contrast variation along the tree-like structure to estimate flow in each vessel. For validating this method we used patient specific software phantoms on which the transport of contrast was simulated. This controlled validation setting enables a direct comparison between estimated flow and actual flow and a detailed investigation of factors affecting accuracy. A total of 10 CCTA image data sets were processed to extract all necessary information for simulating contrast transport. A spectral element method solver was used for computing the ground truth simulations with high accuracy. On this data set, the ADFE method showed a high correlation coefficient of 0.998 between estimated flow and the ground truth flow together with an average relative error of only 1%. Comparing the ADFE method with the best method currently available (TAFE) for image-based blood flow estimation, which showed a correlation coefficient of 0.752 and average error of 20%, it can be concluded that the ADFE method has the potential to significantly improve the quantification of coronary artery blood flow derived from contrast gradients in CCTA images.

KEYWORDS

advection diffusion, blood flow estimation, coronary computed tomography angiography, software phantoms

1 | INTRODUCTION

Coronary computed tomography angiography (CCTA) is conducted by injecting an intravenous iodine based contrast material into the bloodstream to highlight the boundary of the coronary arteries and can be used to anatomically assess the severity of obstructive atherosclerotic plaques, that is, stenoses. CCTA was recently given a Class 1 recommendation with level of evidence of A for patients with stable and acute chest pain in the 2021 American College of Cardiology/American Heart Association guidelines.[1] However, CCTA does not directly provide information about hemodynamics such as flow or pressure loss across the stenosis, which are important functional indicators of Coronary Artery Disease (CAD). An invasive metric that has become the gold standard for evaluating the severity of CAD is Fractional Flow Reserve (FFR), which is calculated as the ratio between the pressure distal to the stenosis and the reference aortic pressure.[2] FFR has been shown to improve patient outcomes, when used to decide whether or not surgical intervention is performed.[3] FFR requires fluoroscopy guided invasive catheterization and the insertion of a pressure wire to a location in the vessel distal to the lesion.

Computational fluid models based on CCTA images are now used in routine clinical practice to noninvasively approximate FFR. The noninvasive analogue of FFR derived from computational fluid dynamics and CCTA images is called FFR_{CT}.[4] In order to calculate FFR_{CT}, the coronary geometry is extracted from the CCTA image and a finite element method is used to solve the equations of fluid flow. The accuracy of this solution depends not only on the spatial resolution and correct segmentation of the coronary vessel lumen but also on the boundary conditions that control the hemodynamic flow rates through each vessel. While geometrical parameters such as coronary artery diameter and myocardial volume can be readily extracted from the CCTA image, boundary conditions are difficult to estimate due to complex, patient-specific physiological conditions. While FFR_{CT} calculated using boundary conditions derived from anatomical information has demonstrated high diagnostic accuracy when compared to FFR,[4] these methods do not leverage the functional information that is implicitly embedded in the CCTA image itself. Recently, there has been growing interest in inferring coronary flows or assessing stenosis severity by analyzing the contrast intensity gradients along the coronary vessels.[5–13] These techniques have the potential to further improve the estimation of boundary conditions and thereby increase the diagnostic accuracy of FFR_{CT}.

Within the aorta, a rise and decay of the concentration of intravenously injected contrast can be indirectly measured via multiple CT acquisitions over time. This rise and fall describes the arterial input function (AIF), which is the concentration of the contrast at the level of the aorta over time. The contrast material is transported by the coronary blood flow (CBF) into the coronary vessels. When the CCTA image is acquired before the peak of the AIF, a linear function can be fitted to the intensities along the paths of the arteries. The slope of this linear function is called the Transluminal Attenuation Gradient (TAG) and is inversely correlated to the blood flow velocity within the same artery: a higher slope relates to a lower flow and vice versa.[6,10,11] Computation of TAG is facilitated by the advent of 256 and 320 row detector CT scanners, such as the Toshiba Aquilion One or GE Revolution, scanners that can image the full heart in a single cardiac cycle ensuring that the error due to sampling over multiple cardiac cycles can be avoided. In recent work, TAG was computed in healthy subjects and patients with CAD[5,6,8,10–12] and was found to be relatively constant across cardiac phases in the left anterior descending (LAD). However, these differences in TAG were significant in the left circumflex (LCx) and right coronary artery (RCA). Moreover, TAG was found to be lower in the RCA -6.5 ± 4.1 HU/cm than in the LAD -13.7 ± 8.0 HU/cm or LCx -12.5 ± 7.8 HU/cm.[11] Park et al. used a phantom study to show that TAG may be affected by vessel tapering which is lower in the RCA compared to the LAD and LCx.[10]

The relationship between TAG and CBF was derived by Eslami et al.[14] by solving the advection diffusion equation. In this work, the effects of diffusion and Taylor dispersion were neglected. Eslami et al. also assumed that the vessel does not change much in cross-sectional area over the path length and that the AIF can be approximated by means of an analytical cosine function. Using these assumptions, they derived a correlation between TAG and CBF called Tomography Transluminal Attenuation Flow Encoding (TAFE) and found a reasonably good correlation between TAFE and CBF measurements using micro spheres on nine canine hearts.[9] TAFE's accuracy on clinical data was validated by Bae et al.,[5] who also introduced the TAFE correlation coefficient k, derived using perfusion CT data, to compensate for the tendency of TAFE to underestimate flow. For the patient group having no occlusions TAFE showed good performance. However, the slope in the correlation lines between TAFE and measured flow in the diseased

patient groups decreased with increasing stenosis severity (1.018 for 0% diameter stenosis, 0.832 for 1%–49% diameter stenosis, 0.819 for 50%–79% diameter stenosis and 0.541 for 70%–99% diameter stenosis).[5]

There are multiple possible explanations for the difference in TAG between healthy and stenosed arteries. Our first hypothesis is that the intensity measured on the CCTA image is not always well correlated with the real concentration of the contrast material. This may be due to low-pass filtering of the measured attenuation in the CCTA reconstruction resulting in contrast blurring outside of the vessel and the partial volume effect. Another hypothesis is that there are dynamic effects caused by diffusion on the contrast concentration that cannot be explained by pure advection.

In previous work, we introduced the Advection Diffusion Flow Estimation (ADFE) method which is an improvement to TAFE in straight axi-symmetric vessels.[15] This improvement is the result of including radial diffusion compared to only advection in the TAFE method. In this paper, we extend and validate the ADFE method for complex patient-specific coronary trees. This is done in a controlled setting, since the intensity measured on the CCTA image is not always well correlated with the real concentration of the contrast material. Under this controlled setting, we again illustrate the critical importance of fundamental diffusion phenomena captured by ADFE that is not directly accounted for in the TAFE methodology.

2 | METHODS

In order for ADFE to compute flow from a CCTA image, several steps are necessary. A schematic of the workflow is shown in Figure 1. This workflow starts from two image data sets obtained during CCTA; the so-called bolus tracking series and the CCTA image itself. The bolus tracking series is acquired before triggering the scanner to image the full 3D CCTA image and consists of single slice images containing the ascending and descending aorta. Its main purpose is tracking the contrast agent over time in order to correctly time the CCTA acquisition when the highest intensity in the coronary vessels is expected. This data set is not used for diagnostic purposes, but can be used for reconstructing the AIF. From the CCTA image, the coronary arteries are segmented and the cross-sectional average intensity from the coronary ostia to the visible outlets are computed. This cross-sectional averaged intensity over the path length representing the spatial data and the AIF representing the temporal data are then input to the ADFE method to estimate the CBF through each vessel.

The controlled workflow used in this paper is shown in the bottom half of Figure 1 with each component described below. Compared to the CCTA workflow, we replaced the CCTA image with patient-specific software phantoms to simulate the transport of the contrast agent. This removes the scanner specific effects on the measured contrast intensity and allows us to directly compare the estimated flow from ADFE with the flow prescribed in the simulation.

2.1 | Patient collective

Patient data used in this study consists of anonymized CT data from 10 patients with suspected coronary artery disease (CAD) who received routine CCTA scans at the Universitair Ziekenhuis Brussel. The scans were retrospectively obtained from a previous study with approval from the local research ethics committee (BUN 143201524614).[16] All scans were performed on a 256-slice CT scanner (Revolution CT, GE Healthcare).

2.2 | Arterial input function

In clinical practice, there are two commonly used methods of timing the CCTA acquisition. The first method is using a test bolus, which is executed by injecting a small volume (mL) of contrast agent with similar injection parameters compared to the actual CCTA scan. The average intensity at the aorta after injection is then tracked and plotted over time. The time until the test bolus reaches maximum intensity has a strong correlation with the time the main bolus reaches a threshold of around 50, 100, 150 or 200 HU.[17,18] This time to peak intensity can, therefore, be used to estimate the acquisition time of the CCTA. The second method is using a bolus tracking mentioned above; in this method, only the main bolus is injected and therefore does not require two scans. Again, the average intensity at the aorta is tracked over time but this is done until a threshold value is reached (around 200 HU) and the scanner will then switch modes to acquire the CCTA.

We obtained bolus tracking data, from the patient data set described in Section 2.1. This data consists of images acquired at multiple time points at the same anatomical position so that both the ascending and descending aorta are

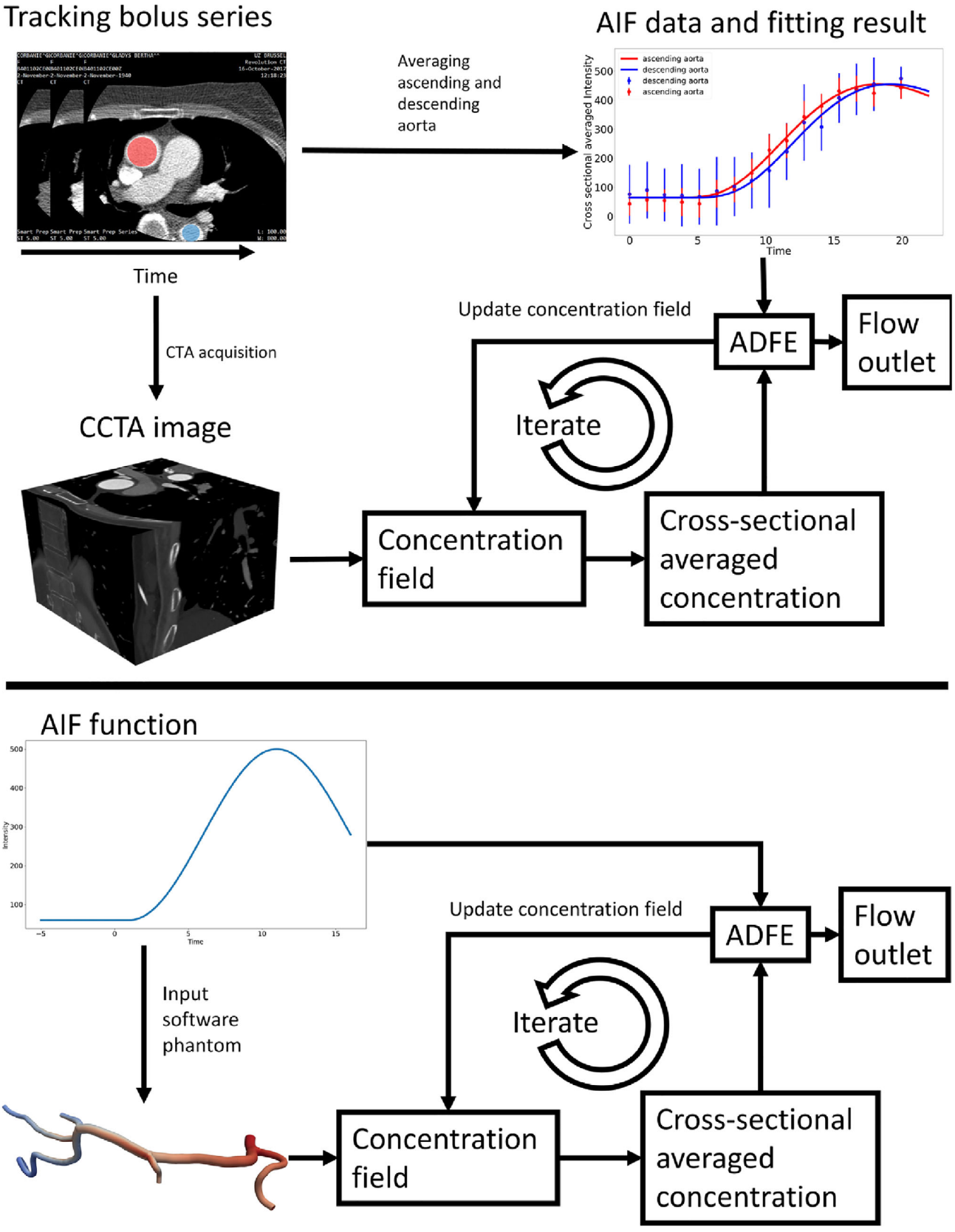

FIGURE 1 Legend on next page.

shown on the images. Time stamps record when the images are acquired. The first time stamp after the start of the injection is set at the zero time point. An image is taken before the injection of the contrast agent is started and a region of interest (ROI) is placed on this image at the ascending aorta. Within this region, the average intensity of the bolus is computed. At the start of the injection, a monitoring delay occurs before the bolus, after which a sequence of single image slices is acquired until the average intensity of the ROI reaches a threshold or a manual start is performed by the operator. The time between each image slice is called the monitor interscan delay. After either reaching the threshold intensity or a manual command to start the scan, the scanner switches modes and pauses until the designated time between the last slice and the actual CCTA scan, called the diagnostic delay, elapses.

To sample the intensities in the ascending and descending aorta, we first segment the aorta on the CCTA and AIF series by placing a seed on the aorta to start a threshold-based region growing algorithm. In certain situations we may also manually segment the aorta. The intensities within the aorta lumen are then extracted and averaged. We then fit an AIF on the combined averaged intensity over time of the ascending and descending aorta. The AIF is parameterized as

$$C(t_n) = C_{max} t_n^{\alpha} e^{\alpha(1-t_n)} + C_0, \text{with} t_n = \frac{t - t_0}{t_m - t_0} \tag{1}$$

where C is the average intensity in HU, C_{max} is the maximal intensity, t is time, t_0 is the time the contrast enters the aorta, t_m is the time the maximal intensity is reached, t_n is the normalized time, $C_0 = C(t_0)$ and α is a parameter that determines the shape of the AIF. This formula is a simplified version of the gamma variate function.[19] In this form, the parameters have no dependencies on each other, thus improving the quality and robustness of the fit, which we performed using least-squares.

2.3 | Patient specific software phantoms

Each patient case is processed by an automated program which segments and labels the myocardium, aorta, and visible coronary arteries from the CCTA image. The centerlines of the segmented aorta and coronary arteries are extracted from the image which includes at each centerline position the tangent-normal vector and the average radius of the corresponding cross-section. Each case includes the three major vessel trees namely the right coronary artery (RCA), left circumflex coronary artery (LCx), and left anterior descending coronary artery (LAD).

2.4 | Spectral element solver

We used a spectral element solver to compute the contrast concentration fields for the software phantoms. This solver was validated and benchmarked in our previous study using 2D axisymmetric meshes.[15] For the volumetric meshes, structured cylindrical segments consisting of 12 elements are created at each centerline point. These 12 elements are placed in such a way that the singularity in the Jacobian caused by mapping a square to a circle is avoided. Additional elements and/or points for higher order elements in the axial direction can then be placed between centerline points. A cubic Hermite spline is used to ensure a smooth transition between two centerline points and their respective tangents.

The Navier–Stokes equations are then solved, treating blood as an incompressible, isotropic, Newtonian fluid. The Neumann resistance boundary conditions at all outlets are based on the coronary geometry and a parabolic velocity

FIGURE 1 (top) Workflow of ADFE for CCTA images. The bolus tracking series is acquired before triggering the scanner to image the full 3D CCTA image. In each bolus tracking image, the ascending (red) and descending (blue) aorta are then segmented and the cross-sectional averaged intensity over time is computed and shown on the plot as dots with error bars indicating the mean and standard deviation of the intensities respectively. Using this sparse data, a continuous parametrized description of the AIF is fitted. This AIF function is then used as input for the ADFE method. Using the 3D CCTA image the coronary arteries are segmented to obtain the concentration field. The cross-sectional averaged intensity over the path length representing the spatial data and the AIF function representing the temporal data are then linked using the ADFE method which does so by estimating the CBF through each vessel. (bottom) Workflow of ADFE for the patient-specific software phantoms, which is used as a proof of concept for the ADFE method. We prescribe a synthetic AIF which serves as input to both the ADFE method and the software phantom. In the software phantom, contrast transport is simulated using this AIF and a three-dimensional velocity field.

profile is prescribed at the inlet of the vessel. The total input flow is scaled on the myocardial mass based on the concept of myocardial supply and demand.[4] Finally, a no-slip boundary condition is prescribed at the lumen wall. With these steady-state boundary conditions, the solver iterates over time until the velocity field converges. After convergence, the velocity field is substituted into the advection diffusion equation. Using the AIF shown in Equation (1), which is used as the boundary condition on the vessel inlet and zero diffusive-flux boundary conditions on all other surfaces, we then calculate the final solution of the concentration field. For post processing, the cross-sectional average value of the concentration field can be computed via numerical integration on the structured mesh.

2.5 | Transluminal attenuation flow encoding

For the derivation of the TAFE method, a scaling analysis was used to justify the use of the 1D advection equation[14]

$$\frac{\partial C}{\partial t}+\frac{Q}{A}\frac{\partial C}{\partial z}=0, \tag{2}$$

with Q is the flow, A is the cross-sectional area and z the axial coordinate. Normalized TAG $G^*_{TA}=\frac{1}{C_{max}}G_{TA}$ is introduced by using the following simplification:

$$G^*_{TA}\approx\frac{1}{C_{max}}\frac{\partial C}{\partial z}. \tag{3}$$

G^*_{TA} is substituted into the 1D advection equation together with the 1D advection solution for the remaining $\frac{\partial C}{\partial t}$ term. Many derivations of Q exist in the TAFE literature each with a slightly different formula for Q based on the assumptions used. In this paper, the clinically tested formulation was used[5,9]:

$$Q=\frac{\widehat{A}\pi}{t_m}\sqrt{\frac{L}{-4G^*_{TA}}}, \tag{4}$$

with $\widehat{A}$ the average area of the vessel and L the vessel length. This single vessel formula was used to compute flow through each outlet by computing G^*_{TA} starting from the inlet of the coronary tree to each outlet. Computing flow through each vessel segment was done by combining these outlet TAFE flows by enforcing conservation of mass.

2.6 | ADFE for coronary trees

The ADFE method was developed for straight axi-symmetric vessels and provides an accurate estimation of the ground truth flow. In the ADFE method a semi-analytical solution of the axi-symmetric advection diffusion is fitted on concentration data by adjusting the amount of flow through the vessel. This semi-analytical solution assumes a parabolic shaped velocity field together with a constant radius of the vessel segment.[15] However, a coronary tree consists of multiple connected vessel segments and on each segment the radius can vary over the vessel path. 3D geometric features, such as curvature, are not explicitly accounted for in the ADFE methodology, and some vessel segments can be too short to reliably fit all parameters independently. This is evident when examining the least square error landscape as the parameters are related and a relative flat minimum exists; this phenomenon is less pronounced with increasing vessel segment length. These errors on individual segments can be largely avoided by linking the vessel segments via the conservation of mass. However, not all segments should have an equal contribution to the total minimization error as this may result in outliers for certain segments in the estimated flow. We use the following two step optimization methodology: First, starting with the semi-analytical solution for the 2D-axisymmetric advection solution described in Bakker et al.,[15] we describe the cross-sectional averaged concentration $\overline{C}$ as function of the nondimensional Peclet number $Pe=Qa^2/DV$ and Strouhal number $St=V/Qt_m$, with Q the flow, a the average radius, D the diffusion coefficient of the solute and V the accumulated volume in the axial direction, in both time t and axial coordinate z. Note that in this work we use the flow notation instead of cross-sectional averaged velocity as the latter is not constant over a

radially varying vessel. All parameters can be measured from the geometry or AIF data except for D and Q. By estimating D we can use the ADFE method to estimate Q. This is done by iteratively minimizing the least-squares error E between the semi-analytical solution and the data by adjusting Q. Setting the boundary conditions in the semi-analytical solution is less trivial compared to the straight single vessels used in our previous work. With the exception of the input vessel, the time-shift t_s in the AIF and concentration input profile g at $z = 0$ is not known for the other vessel segments. Currently we address this by using the concentration profile at the end of the upstream vessel segment and fitting t_s together with Q. Thus starting at the inlet and working downstream, the first step is applying the ADFE method for each vessel segment separately.

In the second and final optimization step, we enforce the conservation of mass by setting the total flow of a vessel segment to be equal to the sum of the downstream vessel segments. This implies that we only need the flow at the outlet vessel segments to calculate the flow on all vessel segments. However, because of the axi-symmetric assumptions underlying the current ADFE method, an outlier in the flow estimation may occur at an outlet vessel segment. We address this issue by defining weights for each segment: for each ith segment $w_i = (\log E_i)^2$ with E_i the error from the first step of the ith segment. The total error is then the sum of all N segments in each tree:

$$E = \sum_{i=1}^{N} w_i E_i. \tag{5}$$

Note that we do not average E_i over the segments to ensure that larger segments contribute more to the total error. Furthermore, w_i is chosen such that the contribution of any single segment does not dominate the total error E, as shorter segments tend to have relatively smaller E_i. Similar to the first step we iteratively minimize E by adjusting each Q at the outlets and t_s at each segment, starting from the optimized values from step one. All minimizations of E are performed using the limited memory Broyden–Fletcher–Goldfarb–Shanno Bounded algorithm available in the SciPy 'minimize' function.[20]

3 | RESULTS

In order to validate the ADFE method for tree-like structures we used the anonymized data described in Section 2.1. The data for each patient included the images used to compute the AIF, as described in Section 2.2. The 3D CCTA image data were segmented and processed to extract the centerline data for creating the volumetric meshes (Section 2.3). The final data set was created by simulating the contrast transport and performing the post processing at a time point where a flattening in the gradient of the AIF occurred, or in other words, the moment the start of the plateau of maximum intensity is reached (Section 2.4). Our tree-based ADFE method and the TAFE method[14] are applied to this set for validation and benchmarking. In total, this data set consist of 366 vessel segments on which the ADFE and TAFE flows could be compared to the ground truth flow. For reference, the measured TAG was on average in the RCA -10.4 ± 5.0 HU/cm, LAD -8.8 ± 5.4 HU/cm and LCX -9.9 ± 7.2 HU/cm which is the same order as reported in Reference [11].

3.1 | AIF example

Two AIF examples from case 1 and 10 are both shown in Figure 2. The AIF from case 1 is a typical example containing a set of data points before arrival of the bolus and a few data points, usually two or three, when the bolus has arrived at the aorta. The last AIF data point was sampled from the actual CCTA image, which was acquired 8 s after the last tracking bolus image, at roughly the same location where the bolus tracking images were acquired.

3.2 | ADFE versus TAFE

We compare ADFE and TAFE by examining the correlation and relative error between Q_m, the flow computed by either ADFE or TAFE, and Q_d, the input flow used to simulate C (Figures 3 and 4). ADFE has an average error of 1% and a

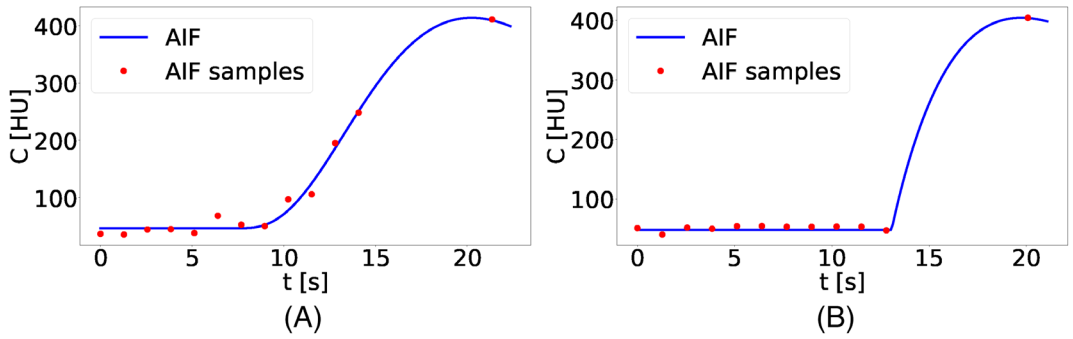

FIGURE 2 AIF examples from case 1 (left) and 10 (right). The red dots are sampled from the corresponding bolus tracking data set at the ascending aorta and the blue line is the corresponding fit of the AIF using Equation (1). The correspondence between this set and the AIF one is excellent.

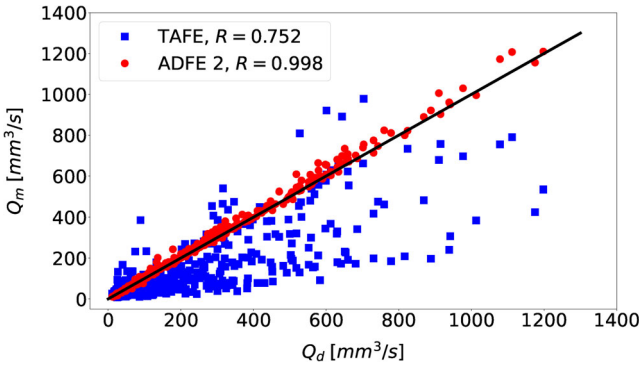

FIGURE 3 Correlation plot between Q_d and Q_m for ADFE (red dots) and TAFE (blue dots) of 366 vessel segments. The correlation coefficient R for each method is shown.

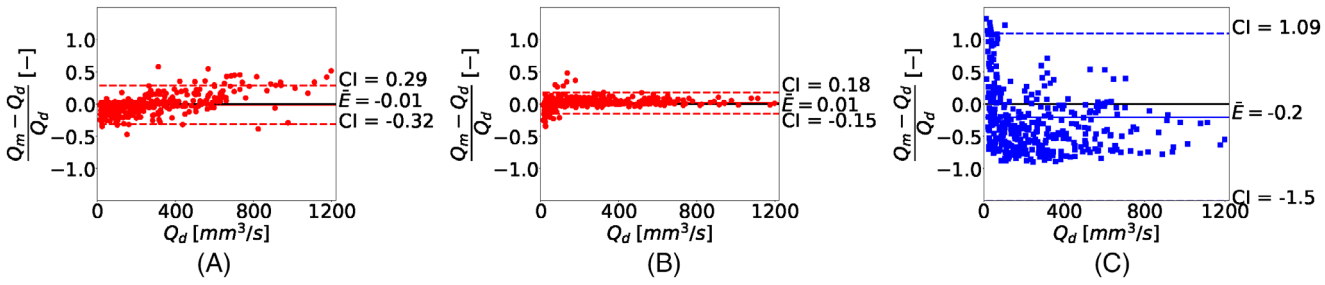

FIGURE 4 Relative difference plots for ADFE first optimization step (A), ADFE second optimization step (B) and the TAFE method (C) of 366 vessel segments. The difference is calculated as $\frac{Q_d - Q_m}{Q_d}$, and for each figure, the mean difference (black line) and 95% confidence interval (dotted line) are shown.

high correlation coefficient $R = 0.998$. The benefit of using the two optimization steps in the tree-based ADFE method is that the relative error changes from -0.015 ± 0.154 after the first step to 0.014 ± 0.084 after the second step. The large improvement in the standard deviation of the relative error is caused by combining information from all vessel segments to mitigate the impact of segments where the single-segment ADFE method results in high error. These are typically segments that conform the least to the axi-symmetric assumptions underlying ADFE or that are too short. TAFE produced a correlation coefficient of 0.752, with a relative error of -0.204 ± 0.662. Q_m computed with ADFE is more accurate compared to TAFE even after the first ADFE optimization step which only uses the single-vessel ADFE method on each segment.

3.3 | Specific cases

Figure 5 shows the ADFE results from the LAD of case 2. A combination of low curvature and straight segments results in a velocity field which aligns well with the assumptions underlying the ADFE method, contributing to high accuracy in the estimated flow. Figure 4B illustrates outliers, that is, data points outside the confidence interval, where the accuracy of ADFE decreases. Two categories of segments exhibited a high relative error. The first category consists of short and relatively low-flow segments that have high curvature. An example of this is the LAD of case 5 shown in Figure 6. In Figure 6, four of these segments are labeled with a different severity of curvature. Specifically, segments 1 and 2 have the largest curvatures with a relative error in the flow estimation of −0.28 and −0.35, respectively. Segments 3 and 4 are straighter vessels comparatively and have lower relative flow errors of −0.11 for both segments. The second category consists of segments with relatively large flows together with large axial variations in radius and curvature. An example of this is the LCx of case 4 shown in Figure 7. From Figure 7A, a good fit between the ADFE concentration solution and the intensity data can be seen. However, the estimated flow still resulted in an overestimation. The cause of the overestimation in this case is due to a nonparabolic velocity field especially in the proximal segments. Due to the high velocity and axially varying geometry, the velocity field becomes more flat and the contrast transport is faster. An overestimation of the ADFE flow is expected due to the parabolic velocity profile assumption of the ADFE method.

4 | DISCUSSION

In this study, we successfully extended the ADFE method from simple axisymmetric vessels[15] to coronary trees. We used patient-specific software phantoms which ensures a fully controlled setting compared to actual CCTA images. The flows estimated by ADFE resulted in a 1% average error compared to the ground-truth flows used in the contrast transport simulations. Central to the ADFE method is the fitting of a semi-analytical solution of the advection diffusion equation to the contrast intensity data, and the tree-based ADFE method relies on a sequence of two optimization steps described in Section 2.6 that leverages information from all of the vessel segments in the coronary tree. Overall, a small standard deviation (8%) in relative error was found in the 10 cases we investigated, which highlights the robustness of

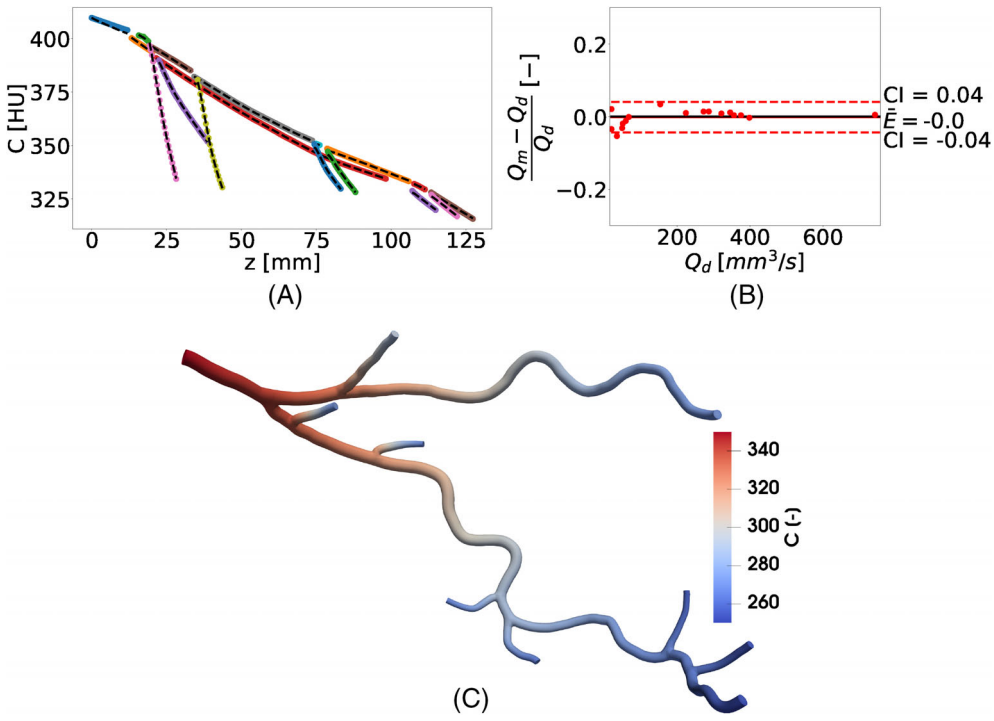

FIGURE 5 ADFE results for the LAD of case 2 with (A) the fit of the semi-analytical solution after the final optimization step for the LAD tree (black dashed lines) and cross-sectional averaged concentration (dotted lines with each color representing a different segment), (B) the relative difference plot for this case and (C) the concentration data present at the surface of the LAD mesh.

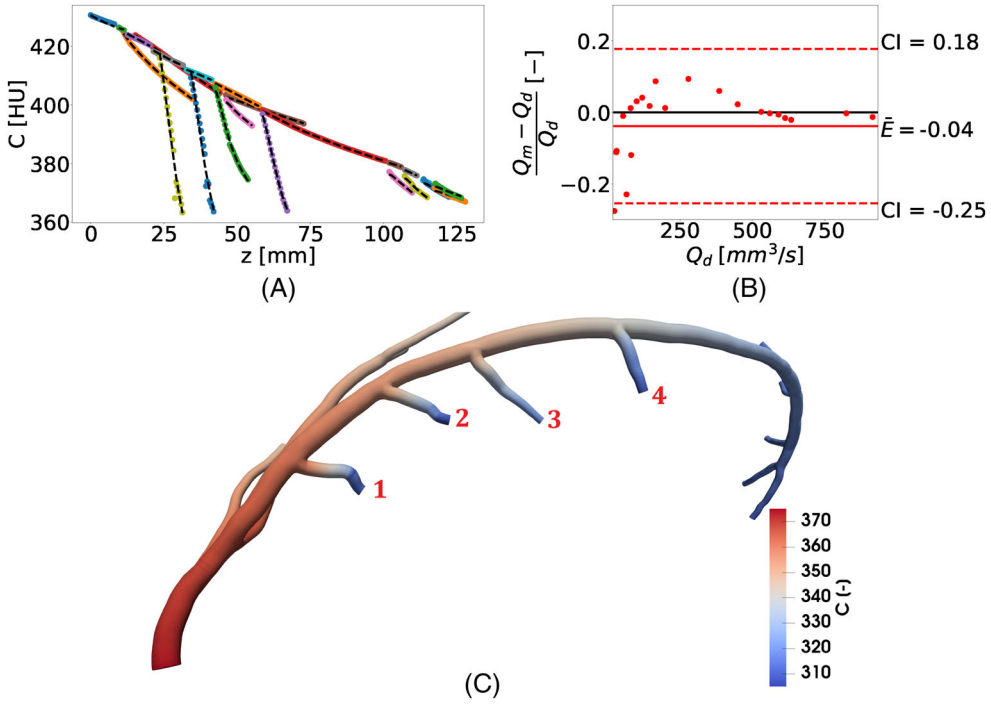

FIGURE 6 ADFE results for the LAD of case 5 with (A) the fit of the semi-analytical solution after the final optimization step for the LAD tree (black dashed lines) and cross-sectional averaged concentration (dotted lines with each color representing a different segment), (B) the relative difference plot for this case and (C) the concentration data present at the surface of the LAD mesh. Additionally four segments are labeled to illustrate the impact of vessel curvature.

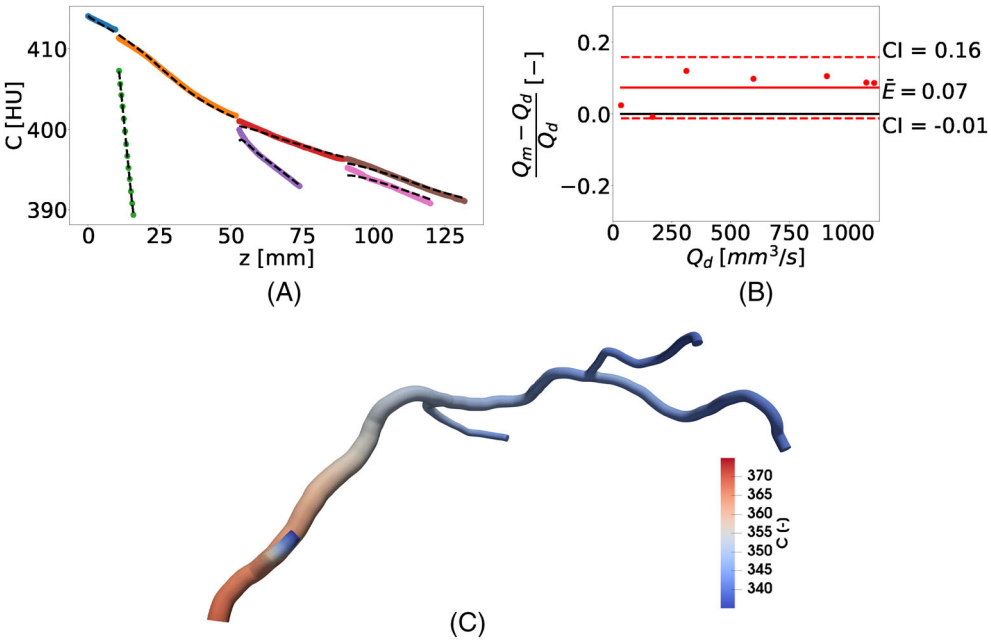

FIGURE 7 ADFE results for the LCx of case 4 with (A) the fit of the semi-analytical solution after the final step for the LAD tree (black dashed lines) and cross-sectional averaged concentration (dotted lines with each color representing a different segment), (B) the relative difference plot for this case and (C) the concentration data present at the surface of the LCx mesh.

the ADFE method. The ADFE method is also fast and computationally inexpensive; the total computation time per case is 1–10 min on a single processing core depending on tree size and convergence criteria.

We have previously compared ADFE with TAFE in axi-symmetric vessels,[15] where we showed significant improvements in accuracy. In this study involving patient-specific coronary vessel trees, the 1% flow estimation error of ADFE was found to be a significant improvement compared to the 20% average error of TAFE. The major difference between ADFE and TAFE is the inclusion of radial transport phenomenon, that is, the velocity profile and radial diffusion that is considered in the ADFE method. In a recent study involving TAFE, a correction for the radial velocity profile has been proposed in the form of a constant correction term.[7] The experimental CCTA setup in this study involved scanning a 3D printed vessel in which a contrast solution was pumped through using different flow rates. Similar to our results, underestimation of the TAFE flow estimate compared to the true flow was found. The correction term resulted in an accurate TAFE flow estimation but the correction is specific to the tested vessel geometry. Choosing a constant correction term would be insufficient for a more general data set as there is a nonlinear relationship between the radial transport and the flow rate. Additionally, TAFE requires the CCTA acquisition to be before the AIF plateau to ensure a negative TAG can measured. In the ADFE method a semi-analytical solution is fitted on the concentration which can be performed at every point in time. Although the greater concentration gradient when acquiring the CCTA before the plateau would improve the robustness of the ADFE fit, it can still be performed when the CCTA timing is off. Overall, we showed that ADFE accurately estimates flow from simulated contrast data extracted from multiple different patient specific coronary vessel trees.

We have identified two distinct situations for which the accuracy of ADFE may decrease. ADFE underestimates flow in small segments with high curvature bifurcating from a relative larger parent vessel. It is possible that this could be the result of numerical artifacts from using a zero diffusive-flux boundary condition at the outlets. However, for these small segments, the absolute flow error in the individual segments is low compared to the total flow of the tree (less than 1%). The second category of outlier segments is where the velocity field significantly differs from the assumed parabolic profile. This is caused by a combination of significant axial variations in radius and a relatively high flow resulting in a flat velocity profile. In these cases, a significant overestimation of the flow may occur. It should also be noted that the coronary trees used in this research are without CAD, which are extreme situations, where this can occur. Special care should be taken when computing ADFE on vessels with CAD, with even excluding the diseased section from the ADFE fit.

Before utilizing ADFE with real CCTA images, additional considerations are necessary. Ideally, fitting the AIF would require more complete temporally resolved image data than is currently available in the investigated cases. Currently the timing images are only used for tracking the arrival of the bolus and timing the actual 3D CT scan. There is a large gap in timing data between the bolus tracking data set and the time of the CCTA scan, and this may result in non-uniqueness of the AIF fit. By reducing the diagnostic delay and extending the bolus tracking, more points could be added on the AIF curve, thus increasing the reliability of the fitted AIF.

Compared to the axi-symmetric vessels in our previous study, realistic AIF data and patient specific geometries were used in the present study to validate the ADFE method for extracting flow from contrast gradients in CCTA images. However, compared to using intensity data from actual CCTA images, we still do not account for important phenomena related to the imaging process and the underlying physiology. The most important consideration with real CCTA images is determining an accurate correlation between the measured image intensity samples from the CCTA images and the actual contrast concentrations. The CCTA imaging process involves blurring, partial volume effects and the presence of imaging artifacts which affect the measured image intensity (HU). Blurring results in a lower measured cross-sectional averaged intensity. The partial volume effect also contributes to lower measured intensities as the intensities of voxels at the lumen boundary which are both inside and outside of the vessel will be averaged out. Correcting these effects is a necessary preprocessing step in utilizing ADFE or TAFE. In their CCTA phantom study the authors of the TAFE method also investigated a correction function based on the area of each cross-section.[7] This was done by scanning a tapered vessel with a constant contrast concentration. Despite the constant concentration, a decreasing intensity along the vessel path was found due to imaging effects correlating with the cross-sectional area. A correction function was then fitted on the ratio between the true constant intensity and measured cross-sectional averaged intensity as a function of the area of each cross-section.

Additionally, the pulsatility in the contrast transport caused by the beating heart is not explicitly accounted for. As the contrast is injected intravenously the contrast is mixed inside the heart chambers and pumped into the aorta, producing oscillations in the AIF. The velocity field is also pulsatile and still developing at the entrance of the coronary

circulation. Both phenomena could be accounted for by adjusting the semi-analytical solution that the ADFE method relies on; more details about this procedure can be found in Bakker et al.[15]

5 | CONCLUSION

We have demonstrated that a tree-based ADFE method can be used to estimate flows on a set of software phantoms based on patient specific geometries with realistic AIF data. This work represents a significant step toward a general and robust method for estimating blood flow from actual CCTA images.

ACKNOWLEDGMENTS

The authors would like to acknowledge HeartFlow, Inc. for providing research funding and Prof. Rajat Mittal for providing insights into the implementation of the TAFE method.

CONFLICT OF INTEREST STATEMENT

N. Xiao, S. Lynch, A. UpdePac, M. Schaap and C. A. Taylor are employees of HeartFlow, Inc.

DATA AVAILABILITY STATEMENT

The data that support the findings of this study are available from the corresponding author upon reasonable request.

REFERENCES

1. Gulati M, Levy PD, Mukherjee D, et al. 2021 AHA/ACC/ASE/CHEST/SAEM/SCCT/SCMR guideline for the evaluation and diagnosis of CHEST pain. *J Am Coll Cardiol*. 2021;78(22):e187-e285. doi:10.1016/j.jacc.2021.07.053
2. Pijls NH, Sels JW. Functional measurement of coronary stenosis. *J Am Coll Cardiol*. 2012;59(12):1045-1057. doi:10.1016/j.jacc.2011.09.077
3. Pijls NH, Fearon WF, Tonino P, et al. Fractional flow reserve versus angiography for guiding percutaneous coronary intervention in patients with multivessel coronary artery disease: 2-year follow-up of the FAME (fractional flow reserve versus angiography for multivessel evaluation) study. *J Am Coll Cardiol*. 2010;56(3):177-184. doi:10.1016/j.jacc.2010.04.012
4. Taylor CA, Fonte TA, Min JK. Computational fluid dynamics applied to cardiac computed tomography for noninvasive quantification of fractional flow reserve: scientific basis. *J Am Coll Cardiol*. 2013;61(22):2233-2241. doi:10.1016/j.jacc.2012.11.083
5. Bae YG, Hwang ST, Han H, et al. Non-invasive coronary physiology based on computational analysis of intracoronary transluminal attenuation gradient. *Sci Rep*. 2018;8(1):4692. doi:10.1038/s41598-018-23134-7
6. Choi JH, Koo BK, Yoon YE, et al. Diagnostic performance of intracoronary gradient-based methods by coronary computed tomography angiography for the evaluation of physiologically significant coronary artery stenoses: a validation study with fractional flow reserve. *Eur Heart J Cardiovasc Imaging*. 2012;13(12):1001-1007. doi:10.1093/ehjci/jes130
7. Eslami P, Seo JH, Rahsepar AA, et al. A noninvasive assessment of flow based on contrast dispersion in computed tomography angiography: a computational and experimental phantom study. *J Biomech Eng*. 2022;144(9):091009. doi:10.1115/1.4053997
8. Fujimoto S, Giannopoulos AA, Kumamaru KK, et al. The transluminal attenuation gradient in coronary CT angiography for the detection of hemodynamically significant disease: can all arteries be treated equally? *Br J Radiol*. 2018;91(1087):20180043. doi:10.1259/bjr.20180043
9. Lardo AC, Rahsepar AA, Seo JH, et al. Estimating coronary blood flow using CT transluminal attenuation flow encoding: formulation, preclinical validation, and clinical feasibility. *J Cardiovasc Comput Tomogr*. 2015;9(6):559-566. doi:10.1016/j.jcct.2015.03.018
10. Park EA, Lee W, Park SJ, Kim YK, Hwang HY. Influence of coronary artery diameter on intracoronary transluminal attenuation gradient during CT angiography. *JACC Cardiovasc Imaging*. 2016;9(9):1074-1083. doi:10.1016/j.jcmg.2015.10.028
11. Steigner ML, Mitsouras D, Whitmore AG, et al. Iodinated contrast opacification gradients in normal coronary arteries imaged with prospectively ECG-gated single heart beat 320-detector row computed tomographys. *Circ Imaging*. 2015;137(9):179-186. doi:10.1161/CIRCIMAGING.109.854307
12. Stuijfzand WJ, Danad I, Raijmakers PG, et al. Additional value of transluminal attenuation gradient in CT angiography to predict hemodynamic significance of coronary artery stenosis. *JACC Cardiovasc Imaging*. 2014;7(4):374-386. doi:10.1016/j.jcmg.2013.12.013
13. Wong DT, Ko BS, Cameron JD, et al. Transluminal attenuation gradient in coronary computed tomography angiography is a novel noninvasive approach to the identification of functionally significant coronary artery stenosis: a comparison with fractional flow reserve. *J Am Coll Cardiol*. 2013;61(12):1271-1279. doi:10.1016/j.jacc.2012.12.029
14. Eslami P, Seo JH, Rahsepar AA, Richard AG, Lardo AC, Mittal R. Computational study of computed tomography contrast gradients in models of stenosed coronary arteries. *J Biomech Eng*. 2015;137(9):091002. doi:10.1115/1.4030891
15. Bakker LMML, Xiao N, Van De Ven AAF, Schaap M, Van De Vosse FN, Taylor CA. Image-based blood flow estimation using a semi-analytical solution to the advection-diffusion equation in cylindrical domains. *J Fluid Mech*. 2021;924:A18. doi:10.1017/jfm.2021.596

16. Van Gompel G, Delombaerde L, Zanca F, et al. A patient- and acquisition-tailored injection approach for improving consistency of CT enhancement towards a target CT value in coronary CT angiography. *J Appl Clin Med Phys*. 2022;24:e13867. doi:10.1002/acm2.13867
17. Platt JF, Reige KA, Ellis JH. Aortic enhancement during abdominal CT angiography: correlation with test injections, flow rates, and patient demographics. *AJR Am J Roentgenol*. 1999;172(1):53-56. doi:10.2214/ajr.172.1.9888738
18. Hoe vL, Marchal G, Baert AL, Gryspeerdt S, Mertens L. Determination of scan delay time in spiral CT-angiography: utility of a test bolus injection. *J Comput Assist Tomogr*. 1995;19(2):216-220. doi:10.1097/00004728-199503000-00009
19. Madsen MT. A simplified formulation of the gamma variate function. *Phys Med Biol*. 1992;37(7):1597-1600. doi:10.1088/0031-9155/37/7/010
20. Virtanen P, Gommers R, Oliphant TE, et al. SciPy 1.0: fundamental algorithms for scientific computing in Python. *Nat Methods* 2020;17:261-272. doi:10.1038/s41592-019-0686-2

How to cite this article: Bakker LMML, Xiao N, Lynch S, et al. Preclinical validation of the advection diffusion flow estimation method using computational patient specific coronary tree phantoms. *Int J Numer Meth Biomed Engng*. 2023;39(9):e3746. doi:10.1002/cnm.3746